AJNR

Erdheim-Chester Disease Mimicking Multiple Meningiomas Syndrome

Mahlon D. Johnson, Joseph P. Aulino, Madan Jagasia and Louise A. Mawn

AJNR Am J Neuroradiol 2004, 25 (1) 134-137
http://www.ajnr.org/content/25/1/134

AJNR Am J Neuroradiol 25:134–137, January 2004

Case Report

Erdheim-Chester Disease Mimicking Multiple Meningiomas Syndrome

Mahlon D. Johnson, Joseph P. Aulino, Madan Jagasia, and Louise A. Mawn

Summary: We describe a rare case of non-Langerhans histiocytosis, consistent with Erdheim-Chester disease (ECD), which presented with lesions resembling multiple meningiomas. The patient was initially evaluated for migraine headaches. Initial MR imaging demonstrated a parasellar mass and a second mass near the torcula considered to represent meningiomas. Within 1 year, he developed bilateral orbital lesions surrounding both optic nerves, which were also considered meningiomas. Biopsy of one orbital mass revealed a non-Langerhans histiocytosis. Subsequently, soft tissue masses, a pericardial effusion, and bone lesions consistent with ECD were identified.

Erdheim-Chester disease (ECD) is a rare non-Langerhans histiocytosis with protean symptoms and involvement of multiple organs, including long bones, skin, lung, soft tissue, and brain (1–7); however, very rare cases present with CNS signs, most commonly diabetes insipidus with or without associated visible hypothalamic lesions (4, 5). Involvement of the dura or orbit is very rare (6, 7).

Case Report

A 34-year-old male patient was initially evaluated for complex migraine headaches. T1-weighted MR imaging with gadolinium revealed two discrete dural-based mass lesions, one in the left parasellar region involving the cavernous sinus extending posteriorly, dorsal to the clivus, with homogeneous enhancement. A second 2.5 × 2.5 cm heterogeneous mass with homogeneous enhancement adjacent to the torcula herophili and appearing epidural in location was also found (Fig 1). These were considered most consistent with meningiomas by their imaging appearance.

Opththamalogic evaluation found visual acuity of 20/20 in each eye, color of 15/15 in each eye, full fields on automated perimetry, and normal ocular motility. Exophthalmometry readings at a base of 104 were 21.5 mm OD and 23 mm OS. Pupils were without evidence of a relative afferent pupil defect, and slit lamp evaluation and posterior pole were normal.

At the time the patient was thought to have a tumor syndrome and was his disease was managed conservatively. MR images 6 months later revealed no change in these masses. At 1-year follow-up, however, the parasellar mass was slightly increased in size. Subsequent evaluation revealed bilateral, similar enhancing intraconal orbital lesions thought to arise from the optic nerve sheaths, which were also considered meningiomas.

The patient was referred to neuro-oncology for review of treatment options and elected to undergo radiation therapy to these lesions. Radiation was then delivered as 50.4-Gy three-dimensional radiation in 28 fractions, completed 2 years after his first headache presentation and 1 year after his initial ophthalmic evaluation.

Over the next year, the patient developed gradual increase in proptosis OS greater than OD, as well as motility deficits OS and a new visual field defect OS. MR imaging revealed a diffuse pachymeningitis most prominently involving the sellar/suprasellar region, the falx cerebri, and the tentorium cerebelli (Fig 2). Both intracranial internal carotid arteries, and the basilar artery became encased by enhancing tissue. Abnormal patchy intra-axial central pontine enhancement with associated T2 hyperintense signal appeared and was thought initially to be ischemic in origin. The orbital disease progressed significantly, and there was nearly complete replacement of the normal intra- and extraconal orbital fat (Fig 2) with significant associated mass effect.

To confirm the diagnosis of menigioma and establish eligibility for a clinical trial, the patient was subjected to an anterior orbitotomy and biopsy of the left orbital mass. This was achieved via an anterior orbitotomy through a lateral canthal incision with a swinging eyelid flap, inferior fornix conjunctival incision. Dissection of the periorbita revealed a firm, white, large nodular mass. Two biopsies were taken.

The samples from the orbital mass were, in aggregate, 2.0 × 1.3 × 1.1 cm of white, extremely firm, fibrous tissue. Intraoperative analysis revealed a lesion consistent with a benign fibrous tumor. Permanent sections revealed a fibrous tumor with an extensive, predominantly histiocytic infiltrate without giant cells, emperipolesis or necrobiosis (Fig 3). No Reed-Sternberg or lacunar cells were found, and eosinophils were rare. The histiocytes exhibited CD68, α-anti-chymotrypsin, and rare S-100 protein, but no CD1a immunoreactivity. Occasional, nondysplastic plasma cells and CD3 or CD20 immunoreactive, small nontransformed lymphocytes were also found. No meningothelial histology and no epithelial membrane antigen or cytokeratin immunoreactivity were found. A diagnosis of non-Langerhans histiocytic lesion was made. Considered with the clinical and radiographic features, these lesions were consistent with manifestations of ECD. Recently it has been suggested that chronic myeloproliferative disorders and possibly non-Langerhans histiocytic lesions with translocations between chromosomes 5 and 12 resulting in overexpression of the platelet-derived growth factor (PDGF) receptor-β might respond to imatinib mesylate (Gleevec) therapy. Imatinib mesylate is an inhibitor of the PDGF receptor tyrosine kinase (8). Thus, fluorescence in situ hybridization analysis was performed by using 5q33–34 probes (PDGFR and CSF1R) 5p15.2 (LSI D5S23 and D5s721), 12p13(TEI/ETV6), and 21q22 (AML1 gene). This revealed no monosomy 5, 5q deletion, monosomy 7, 7q deletion, or 5:12 translocation.

Subsequent examination revealed no cervical adenopathy. Postgadolinium T1-weighted MR imaging of the chest revealed a mildly enhancing soft tissue lesion surrounding the superior aspect of the aortic arch with extension along the left subclavian artery. Similar findings were seen along the abdominal aorta. A pericardial effusion was also identified and subse-

Received February 3, 2003; accepted after revision April 10.

From the Departments of Pathology (M.D.J.), Radiology and Radiological Sciences (J.P.A.), Hematology and Oncology (M.J.), and Ophthalmology (L.A.M.), Vanderbilt Medical School, Nashville, TN.

Address correspondence to Dr. Mahlon D. Johnson, Department of Pathology, Vanderbilt Medical School, 21st Ave. S, Nashville, TN 37232.

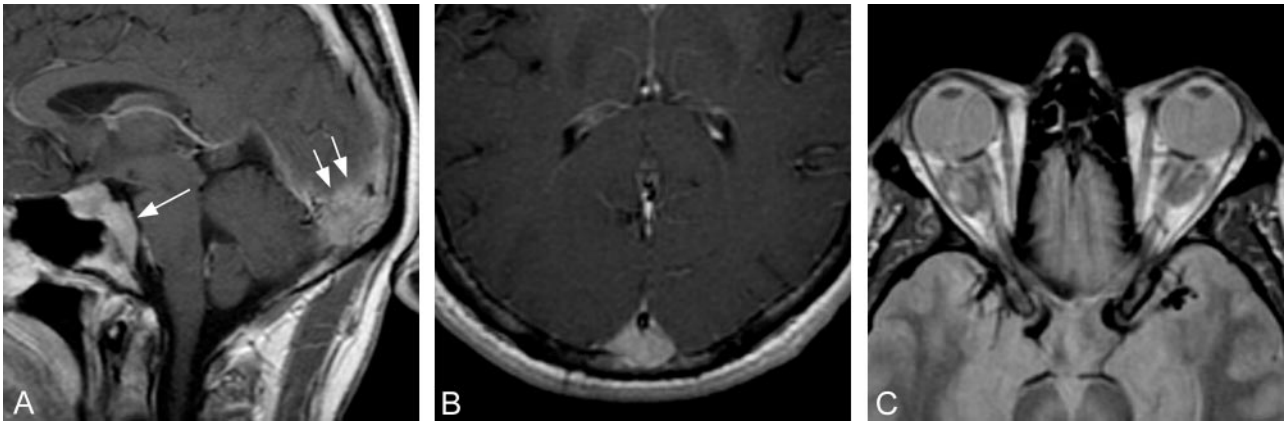

FIG 1. Selected MR images through the head and orbits obtained at initial presentation, 3 years before histologic diagnosis.

A, Sagittal T1-weighted postcontrast image shows abnormal homogeneous enhancement extending posteriorly from the sella, along the clivus (*single arrow*). There is a 2.5-cm enhancing epidural mass seen at the level of the torcula (*double arrows*).

B, Axial T1-weighted postcontrast image reveals a focal enhancing epidural lesion displacing the posterior portion of the superior sagittal sinus anteriorly.

C, Axial proton attenuation-weighted image through the orbits shows hypointense bilateral intraconal mass lesions.

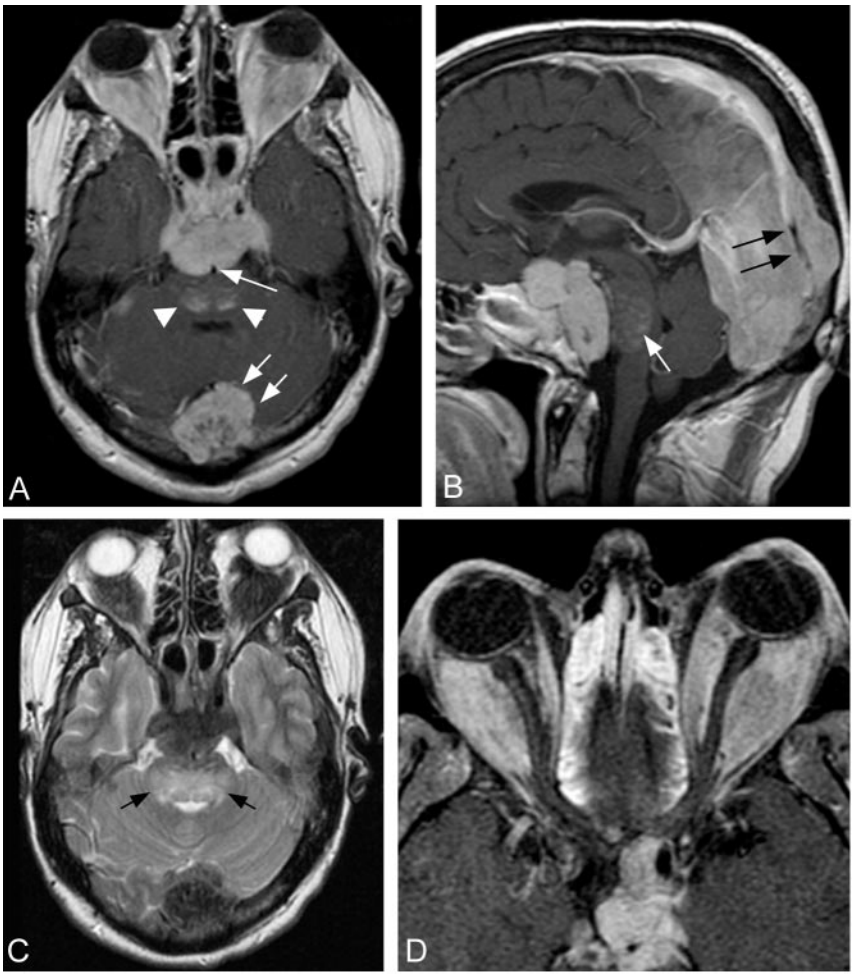

FIG 2. Selected MR images obtained through the brain and orbits 3.0 and 2.5 years after presentation, respectively.

A, Axial T1-weighted postcontrast image through the level of the sella shows a homogeneously enhancing sellar mass lesion extending posteriorly encasing the basilar artery (*single arrow*). Lateral extension encases the cavernous internal carotid arteries. Patchy enhancement is present within the dorsal aspect of the pons (*arrowheads*). There has been a significant interval increase in size of the enhancing midline epidural lesion identified at the level of the torcula (*double arrows*).

B, Sagittal midline postcontrast image shows significant compression of the pons by the prepontine component of the sellar mass. Hazy enhancement within the pons is visualized (*white arrow*). The posterior falx cerebri is thickened, and the posterior aspect of the superior sagittal sinus is encased by enhancing tissue (*black arrow*).

C, Axial T2-weighted image obtained through the level of the fourth ventricle reveals confluent hyperintense signal intensity within the central and dorsal pons (*arrows*). The sellar and torcula mass lesions, as well as the intraconal orbital masses, are markedly hypointense.

D, Axial T1-weighted fat-suppressed postcontrast image through the orbits shows diffuse replacement of the intraconal fat by the large, homogeneously enhancing orbital masses. Patchy enhancement within the ethmoid sinuses reflects sinus disease, not considered a component of the patient's disease burden.

quently drained, revealing 400 mL of clear fluid, which contained chronic inflammatory cells. MR images of the femurs revealed mild osteopenia. MR imaging of the spine 6 months later showed focal L5 abnormal vertebral body marrow signal intensity and no evidence of dural spinal disease. Whole-body ^{18}FDG-PET imaging revealed marked hypermetabolic activity within the orbit and dural masses and within the pons.

Discussion

Although ECD affects many organ systems, patients usually present with symptoms of appendicular skeleton involvement (3). Histiocytic infiltration of long bone metaphyses usually manifests a sclerotic

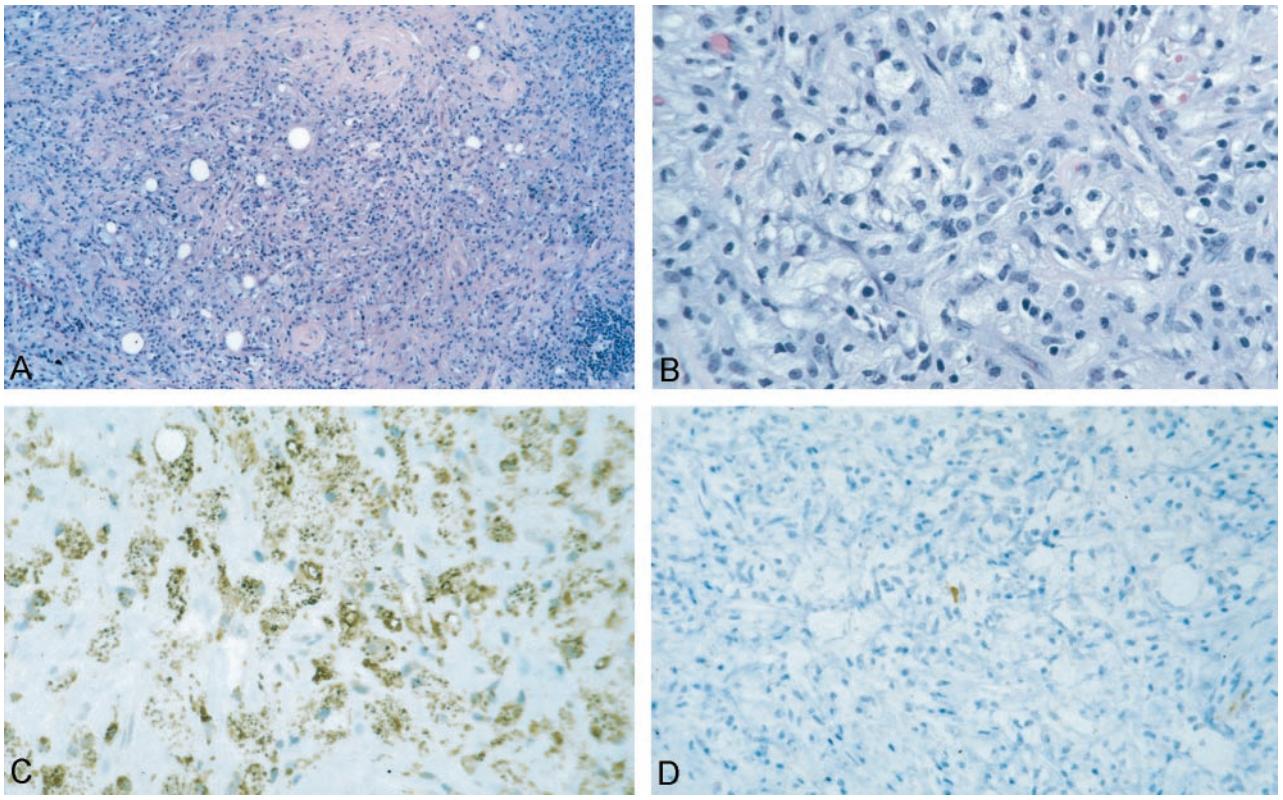

FIG 3. Non-Langerhans histocytosis.
A, Histiocytic and chronic inflammatory lesion with extensive fibrosis.
B, Much of the lesion was foamy histiocytes without emperipolesis or giant cells.
C and *D,* Tumor cells exhibited extensive CD68 (*C*) but only extremely rare S-100 protein (*D*) and no CD1a immunoreactivity.

appearance on conventional radiographs and CT scanning, with typical sparing of the epiphyses, and there is corresponding increased uptake of radiotracer by skeletal scintigraphy. MR imaging reveals patchy metaphyseal T2-hyperintense signal with fat-suppression techniques (9). Symmetric involvement of the appendicular skeleton is usual. Other organ systems and tissues may be involved, including the kidneys, retroperitoneum, lungs, pleura, pericardium, heart, blood vessels, axial skeleton, and skin (9, 10).

ECD rarely involves the CNS. When it does, involvement centers at the hypothalamus, producing diabetes insipidus in one-third of patients, although a mass lesion affecting the sella or hypothalamus is not always visible (4, 5). Involvement of the orbit has also been reported but may reflect extension along the optic nerves from a hypothalamic/chiasmal lesion (6, 7). Dural involvement usually manifests as dural mass lesions, often affecting the falx cerebri, cerebellar tentorium, and sellar region (4). These dural lesions enhance after contrast material administration, with both MR and CT imaging.

Intraconal orbital mass lesions may be bilateral, appearing to arise from the optic nerve sheath. These dural lesions enhance after contrast material administration, both with MR and CT imaging. An unusual feature of these lesions is there persistent enhancement for 2 or more weeks after intravenous Gd-DTPA infusion. This is thought to be caused by uptake of Gd-DTPA by abnormal histiocytes (11, 12).

Clinical and radiologic features of this case, reviewed at several academic centers, were felt to be consistent with multiple meningiomas. Production of meningioma-like tumors in ECD, although extremely rare, has been reported (5). Nonetheless, the development of multiple meningioma-like masses in one patient mimicking neurofibromatosis type II has not been described, to the best of our knowledge. Leptomeningeal ECD must be distinguished from Langerhans histiocytosis and a number of inflammatory lesions with histiocytes that can produce meningioma-like masses in the leptomeninges. These include Rosai-Dorfman disease (RDD), plasma cell granulomas, neurosarcoidosis, and xanthogranulomas (13). In contrast to Langerhans histiocytosis, lesions of ECD are populated by histiocytes without nuclear grooves that show CD68 but little or no S-100 and no CD1a immunoreactivity. Bierbeck granules are also absent. Dural RDD contains histiocytes that are extensively S-100 immunoreactive but are CD1a negative, and lack striking nuclear grooves and Bierbeck granules ultrastructurally. Moreover, RDD exhibits a lymphocytic emperipolesis not seen in other entities. Plasma cell granulomas may present as a similar dural-based mass but histologically are populated primarily by a polytypic population of mature plasma cells, plasmacytoid and small nontransformed lymphocytes in a background of variable fibrosis, and relatively few S-100 immunoreative histiocytes Russell bodies are usually present (13). In contrast to

ECD, pseudomeningiomatous neurosarcoid is overtly granulomatous with multinucleated giant cells and epitheliod histiocytes that react with antibodies to MAC 387 and CD68 but not with S-100 protein. Limited numbers of lymphocytes and plasma cells are present, and there is extensive fibrosis. Schaumann or asteroid bodies may or may not be seen in giant cells and are not specific for sarcoid.

An unusual feature of this case is the presence of a meningioma-like mass at the torcula. Although to the best of our knowledge this has not been described previously, involvement of the cerebellum with associated ataxia has been (14, 15). Most cerebellar and brain stem lesions reported have been histiocytic infiltrates with or without demyelination, rather than circumscribed mass lesions (14, 15).

Conclusion

We describe a case of ECD presenting as multiple extraaxial lesions that appeared similar to meningiomas involving the parasellar region, torcula, and orbits. This entity should be considered in cases of multiple dural lesions.

References

1. Tien R, Kucharczyk J, Newton TH, et al. **MR of diabetes insipidus in a patient with Erdheim-Chester disease: case report.** *AJNR Am J Neuroradiol.* 1990;11:1267–1170
2. Caparros-Lefebvre D, Pruvo JP, Remy M, et al. **Neurologic aspects of Erdheim-Chester disease.** *AJNR Am J Neuroradiol* 1995;16: 735–740
3. Veussier-Belot C, Coud P, Caparros-Lefebvre D, et al. **Erdheim-Chester disease clinical and radiological characteristics of 59 cases.** *Medicine* 1996;75:157–169
4. Babu RP, Lansen TA, Chadburn A, et al. **Erdheim-Chester disease of the central nervous system: report of two cases.** *J Neurosurg* 1997;86:888–892
5. Wright RA, Hermann RC, Parisi JE. **Neurological manifestations of Erdheim-Chester disease.** *J Neurol Neurosurg Psychiatry* 1999;66: 72–75
6. Alper MG, Zimmerman LE, La Pinna FG. **Orbital manifestations of Erdheim-Chester disease.** *Trans Am Opththamol Soc* 1983;81: 64–85
7. Shields JA, Shields CL. **Clinical spectrum of histiocytic tumors of the orbit.** *Trans Pa Acad Ophthalmol Otolaryngol* 1990;42:931–937
8. Savage DG, Antman KH. **Imatinib mesylate: a new oral targeted tharapy.** *N Engl J Med* 2002;346:683–692
9. Breuil V, Brocq O, Pellegrino C, et al. **Erdheim-Chester disease: typical radiological bone features for a rare xanthogranulomatosis.** *Ann Rheum Dis* 2002;61:199–200
10. Egan AJ, Boardman LA, Tazelaar HD. **Erdheim-Chester disease: clinical, radiologic, and histopathologic findings in five patients with interstitial lung disease.** *Am J Surg Pathol* 1999;23:17–26
11. Tien RD, Brasch RC, Jackson DE, Dillon WP. **Cerebral Erdheim-Chester disease: persistent enhancement with GD-DTPA on MR images.** *Radiology* 1989;172:791–792
12. Kujat C, Junk B, Hermes M, et al. **Zerebrale manifestation der Erdheim-Chester-Krankheit.** *Radiologe* 1991;31:307–309
13. Johnson MD, Powell SZ, Boyer PJ, et al. **Dural masses mimicking meningiomas.** *Hum Pathol* 2002;12:1211–1226
14. Fukazawa T, Tsukishima E, Sasaki H, et al. **Erdheim-Chester disease and slowly progressive cerebellar dysfunction.** *J Neurol Psychiatry* 1995;58:238–240
15. Evidente VG, Adler CH, Giannini C, et al. **Erdheim-Chester disease with extensive intraaxial brain stem lesions presenting as a progressive cerebellar syndrome.** *Mov Disord* 1998;13:576–581